

# Rayleigh wave for detecting debonding in FRP-retrofitted concrete structures using piezoelectric transducers

H. Mohseni<sup>a</sup> and C. T. Ng<sup>\*</sup>

*School of Civil, Environmental and Mining Engineering, The University of Adelaide, Adelaide, SA 5005, Australia*

*(Received July 25, 2017, Revised August 10, 2017, Accepted August 19, 2017)*

**Abstract.** Applications of fibre-reinforced polymer (FRP) composites for retrofitting, strengthening and repairing concrete structures have been expanded dramatically in the last decade. FRPs have high specific strength and stiffness compared to conventional construction materials, e.g., steel. Ease of preparation and installation, resistance to corrosion, versatile fabrication and adjustable mechanical properties are other advantages of the FRPs. However, there are major concerns about long-term performance, serviceability and durability of FRP applications in concrete structures. Therefore, structural health monitoring (SHM) and damage detection in FRP-retrofitted concrete structures need to be implemented.

This paper presents a study on investigating the application of Rayleigh wave for detecting debonding defect in FRP-retrofitted concrete structures. A time-of-flight (ToF) method is proposed to determine the location of a debonding between the FRP and concrete using Rayleigh wave. A series of numerical case studies are carried out to demonstrate the capability of the proposed debonding detection method. In the numerical case studies, a three-dimensional (3D) finite element (FE) model is developed to simulate the Rayleigh wave propagation and scattering at the debonding in the FRP-retrofitted concrete structure. Absorbing layers are employed in the 3D FE model to reduce computational cost in simulating the practical size of the FRP-retrofitted structure. Different debonding sizes and locations are considered in the case studies. The results show that the proposed ToF method is able to accurately determine the location of the debonding in the FRP-retrofitted concrete structure.

**Keywords:** FRP-retrofitted concrete structures; structural health monitoring; debonding; Rayleigh wave; finite element simulation; guided wave; absorbing layer

## 1. Introduction

Structural health monitoring (SHM) involves the implementation of damage detection techniques to structures (Raghavan and Cesnik 2007, Worden *et al.* 2007, Ng and Chan 2014). Engineering infrastructures are indispensable assets of the society and provide people with essential services. Therefore, the paramount importance of SHM has been widely recognised. Among different damage detection methods, guided wave-based approach has emerged as a promising technique (Diamanti *et al.* 2004, Schubert *et al.* 2014, Ng 2015b, Tian *et al.* 2015, He and Ng 2017a, Aryan *et al.* 2017b). Guided waves propagate in solid media, interacting with the boundaries in such a way that boundary conditions could be satisfied. Different types of guided waves can occur depending on geometrical properties and boundary conditions of the structure (Mohabuth *et al.* 2016, He and Ng 2017b, Yang *et al.* 2018).

Rayleigh wave propagates on the surface of a semi-infinite solid medium. Lamb waves propagate in plate-like

structures and their propagation is guided by the free upper and lower surface boundaries of the plate (Ng 2015a). Compared to conventional bulk wave methods, guided wave-based damage detection techniques offer some advantages, such as relatively long travel distances, active nature in damage detection, high sensitivity to small damages, capability to inspect inaccessible locations and feasibility of embedding in structural components (Ng 2014a, b, Carboni *et al.* 2015, Harb and Yuan 2015, He and Ng 2015).

### 1.1 Guided waves in composites

Guided wave-based damage detection techniques in composites have been studied extensively in the last two decades (Aryan *et al.* 2017a, Raghavan and Cesnik 2007, He and Ng 2016). Rose (2002) provided an insight on the potentials of guided waves for SHM by outlining advantages of guided waves along with possible application fields. Delamination is one of the common types of damage in composite laminates; therefore, it is important to extract characteristics of scattered guided wave signals from the delamination. Because of multi-layered and non-isotropic nature of composite laminates, guided wave propagation in composite laminates is complex (Soleimanpour and Ng 2017a). It is very challenging to extract the information of the presence of delamination from the measured signals (Chakraborty 2009). Ramadas *et al.* (2009) presented

---

\*Corresponding author, Senior Lecturer

E-mail: alex.ng@adelaide.edu.au

<sup>a</sup>Ph.D. Student

E-mail: hasan.mohseni@adelaide.edu.au

numerical simulations and experimental verification for interaction of fundamental anti-symmetric mode of Lamb wave ( $A_0$ ) at delaminations located symmetrically in the through-thickness direction of composite laminates. After that, Ramadas *et al.* (2010) also investigated the interaction of fundamental symmetric mode of Lamb wave ( $S_0$ ) and  $A_0$  Lamb wave at delaminations located asymmetrically in the through-thickness direction. Singh *et al.* (2012) presented a numerical approach to model the interaction of  $A_0$  Lamb waves with delamination in glass fibre-reinforced composite laminates.

### 1.2 Damage detection techniques for FRP-retrofitted concrete structures

Fibre reinforced polymer (FRP) composites have been extensively used to increase flexural and/or shear strength, improve ductility and repair damaged and deteriorated concrete structures (Biolzi *et al.* 2013, Choi *et al.* 2013, D'Antino and Pellegrino 2014). The need for retrofitting may arise from errors in design and/or construction and higher loading requirements (Balaguru *et al.* 2009, Bank 2006). FRPs have high strength-to-weight and stiffness-to-weight ratios compared to conventional retrofitting materials, e.g., steel. Ease of installation with minimum labour and equipment cost, versatile fabrication and tailorable mechanical properties are the other advantages of FRP composites. FRPs also have good resistance to corrosion (Ko *et al.* 2014).

There are, on the other hand, serious concerns about sustainability of FRP composites in civil engineering applications (Alampalli and Ettouney 2014). Defects in FRP-rehabilitated concrete structures can occur in constituent materials (fibre and epoxy resin), during preparation and installation of FRP on concrete substrate, or during their service life (Karbhari *et al.* 2005). Human errors, flawed or inadequate procedures and environmental factors can contribute to occurrence and propagation of defect in FRP-rehabilitated concrete structures (Akuthota *et al.* 2004). If defects are undetected and untreated, effectiveness of the retrofitting and performance of the FRP-retrofitted concrete elements can be adversely affected (Nassr and Dakhakhni 2009, Xu *et al.* 2005). Therefore, SHM needs to be implemented in FRP-retrofitted concrete structures with proper damage detection techniques.

A number of non-destructive evaluation (NDE) techniques have been used for detecting defects in the FRP-retrofitted concrete structures. Visual inspection is the first and basic step in any structural safety inspection. Some types of defects in the FRP-retrofitted concrete structures, such as UV-induced material discoloration, surface moisture absorption and fabric wrinkles can be detected by visual inspection (Nishizaki and Meiarashi 2002). However, visual inspection is susceptible to misunderstanding of the inspector, especially in varying inspection conditions. Also, visual inspection is not capable of finding sub-surface defects in the FRP-retrofitted concrete structures (Khan 2010). Impact testing, also known as hammer tapping, is another simple method for finding debondings in the FRP-retrofitted concrete structures (Washer and Alampalli 2014a). It involves the use of a hard object, such as hammer

to impact the surface of the composite material bonded on a concrete substrate. Debonding between FRP composite and concrete could result in a distinctive tone. Although impact testing is a very simple method, it is highly subjective, time-consuming and does not show a good level of consistency (ACI 440R-07).

Infrared thermography (IRT) is another NDE technique for the FRP-retrofitted concrete structures (Brown and Hamilton 2013). It involves flowing heat through the inspection area. Existence of a defect can disrupt the flow, resulting in surface temperature change and this can be captured by an infrared camera (Washer and Alampalli 2014b). There are several drawbacks regarding IRT method. The presence of dirty or wet surfaces can make the IR thermal image very noisy, i.e., hiding subsurface defects. Furthermore, IRT is highly sensitive to environmental factors, such as sunshine, wind and ambient temperature (Ettouney and Alampalli 2012). Moreover, emissivity could vary from material to material, which could affect the consistency of results (Turatsinze *et al.* 2011). Another damage detection technique in the FRP-retrofitted concrete structures is acoustic emission (AE). It is based on the fact that when structural elements undergo certain levels of stress, acoustic bursts are released from the material if defects appear in the structure (Mirmiran *et al.* 1999). AE can be used to detect debonding between FRP and concrete substrate (Fam and Mirmiran 2014). The main disadvantage of acoustic emission is that it is a passive method, i.e. the structure needs to be loaded to a certain level and defect must exist so that sensors could capture the acoustic emissions (Karbhari *et al.* 2005).

A number of studies have focused on detection of debonding between FRP and concrete using piezoelectric ceramic (PZT) elements. PZT elements are one of the most commonly used transducers in SHM (Raghavan and Cesnik 2007). PZT function is based on direct and inverse piezoelectric effects. The piezoelectric direct effect is the generation of electric charge due to mechanical stress. The opposite effect, is the application of a difference of potential to induce strain (Cheeke 2012). Therefore, PZT can function as both actuator and sensor. Jiang *et al.* (2017) studied on detection of debonding between FRP bar and concrete structure using PZT transducers and wavelet packet analysis. Sun *et al.* (2015) presented an impedance-based method to detect debonding in concrete beams strengthened with FRP strips using PZT sensor/actuators. An ensemble particle swarm optimization approach was also adopted to improve the accuracy of debonding detection method. Sevillano *et al.* (2016) studied on sensing methods for debonding detection in reinforced concrete beams strengthened with externally-bonded FRP strips. Fibre Bragg grating (FBG) sensors were compared with PZT sensors in this study. Debonding detection in concrete-filled FRP tubes was studied by Luo *et al.* (2016) using time-of-flight (ToF) of ultrasonic waves generated by PZT transducers.

### 1.3 Rayleigh wave for SHM in FRP-retrofitted concrete structures

To date, Rayleigh wave has been studied for detecting

surface and near-surface defects and evaluating repairs in concrete structures. Hevin *et al.* (1998) presented a numerical model for characterisation of concrete surface crack using Rayleigh wave. Edwards *et al.* (2006) worked on gauging of concrete surface crack depth using wideband Rayleigh waves. Zerwer *et al.* (2005) studied on Rayleigh wave-based surface crack detection in concrete with numerical and experimental measurements. Shin *et al.* (2007) worked on improving velocity measurement of Rayleigh wave for NDE of early-age concrete. Concrete surface cracks could be repaired by injection of epoxy materials. Aggelis and Shiotani (2007) worked on evaluating repair of concrete surface cracks by Rayleigh waves. Aggelis *et al.* (2009) studied the relationship between Rayleigh wave characteristics and the depth of concrete surface cracks. An experimental work was presented by Sun *et al.* (2008) by analysing Rayleigh wave parameters for damage detection in concrete structures.

Considering the limitations of current damage detection methods, applications of Rayleigh wave have the potential for active and real-time monitoring of the FRP-retrofitted concrete structures using embedded actuating/sensing system. This paper aims at developing a ToF approach using Rayleigh wave to detect and locate debonding at the interface of FRP and concrete in the FRP-retrofitted concrete structures.

The paper is organised as follows. A three-dimensional (3D) finite element (FE) model for simulating Rayleigh wave propagation and scattering debonding is described in Section 2. Absorbing layers for Rayleigh wave in the FRP-retrofitted concrete structures are then presented. After that, the proposed ToF method for locating debonding in FRP/concrete is presented. The 3D FE model for simulating Rayleigh wave propagation in the FRP, concrete and FRP-retrofitted concrete structures is verified in Section 3. Then, different debonding cases are used to demonstrate the capability of the proposal debonding detection method. Finally, conclusions are drawn in Section 4.

## 2. Methodology

### 2.1 Finite element simulation

In this study, 3D FE simulations are performed using ABAQUS/Explicit. The simulation results are then used to verify the proposed ToF damage detection approach described in Section 2.4. The FE simulations involve modelling of FRP-retrofitted concrete, excitation of Rayleigh wave and calculation of the scattered wave signals from the debonding.

Four-noded S4R shell elements are used to model the FRP laminate and eight-noded C3D8R solid elements are used to model the concrete. Preliminary simulation results with and without rebars in the concrete show that the rebars in the concrete has minor effects on the measured Rayleigh wave and only cause body wave reflections, which could be removed by baseline subtraction. Effects of rebars on Rayleigh wave scattering from debonding is discussed in Section 3.3. Therefore, the rebars are not modelled in the FE model in this study. In the literature, it was shown that

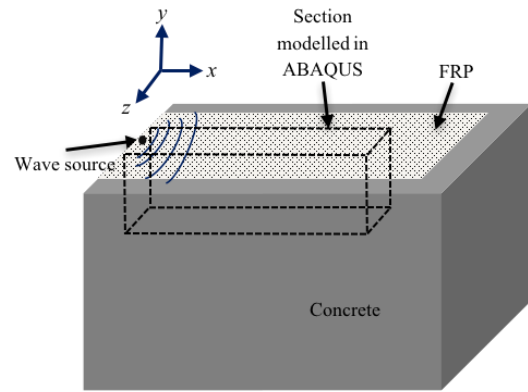


Fig. 1 Schematic diagram of FRP/concrete model

Table 1 Elastic properties of fibre and epoxy matrix

Elastic properties of carbon fibre					
$E_{f11}$ (GPa)	$E_{f22}$ (GPa)	$G_{f12}$ (GPa)	$G_{f23}$ (GPa)	$\rho_f$ (kg/m <sup>3</sup> )	$\nu_{f12}$
231	14.48	22.75	4.83	1760	0.27
Elastic properties of epoxy matrix					
$E_m$ (GPa)	$G_m$ (GPa)	$\rho_m$ (kg/m <sup>3</sup> )	$\nu_m$		
3.77	1.35	1220	0.40		

limiting the excitation frequency up to 150 kHz could minimise the Rayleigh wave scattered from concrete aggregates (Wu and Chang 2006). Thus, a 150 kHz narrow-band five-cycle sinusoidal tone burst pulse modulated by a Hanning window (Hedayatrasa *et al.* 2016) is used as the excitation signal. The Rayleigh wave is generated by applying out-of-plane nodal displacement to the FE nodes covered by a 10 mm diameter circular transducer area. It should be noted that the actual body of transducer was not modelled in ABAQUS simulations. The Rayleigh wave was measured by monitoring out-of-plane nodal displacements.

Shell elements with dimension 1 mm×1 mm and solid elements with dimension 1 mm×1 mm×1 mm are used in ABAQUS models. This ensures at least 12 FE nodes exist per wavelength, and hence, guarantees the accuracy of the FE simulations. The stable time increment is automatically controlled by ABAQUS. To simulate the FRP-retrofitted concrete, surface-to-surface tie constraint is applied to connect nodes between the shell and solid elements. For numerical case studies, the debonding between FRP and concrete is simulated by untying nodes covered by the debonding area. Since the element size is usually very small compared to the actual size of the concrete element, simulation of wave propagation in the whole concrete element will result in a large number of elements in the model, i.e., expensive computational cost. To overcome this issue in the numerical case studies, only a section of FRP-retrofitted concrete structure is modelled in ABAQUS as shown in Fig. 1. Since the wave propagation is a local phenomenon, this section can represent a large FRP-retrofitted concrete structure with the use of absorbing regions described in Section 2.3.

The FE simulation results are verified using DISPERSSE program (Pavlakovic and Lowe 2003). DISPERSSE is based on the global matrix method to calculate the dispersion

Table 2 Elastic properties of FRP ply

$E_{11}$ (GPa)	$E_{22}$ (GPa)	$E_{33}$ (GPa)	$G_{12}$ (GPa)	$G_{13}$ (GPa)	$G_{23}$ (GPa)
170.78	10.30	10.30	6.97	6.97	3.53
	$\nu_{12}$	$\nu_{13}$	$\nu_{23}$	$\rho$ (kg/m <sup>3</sup> )	
	0.30	0.30	0.46	1617	

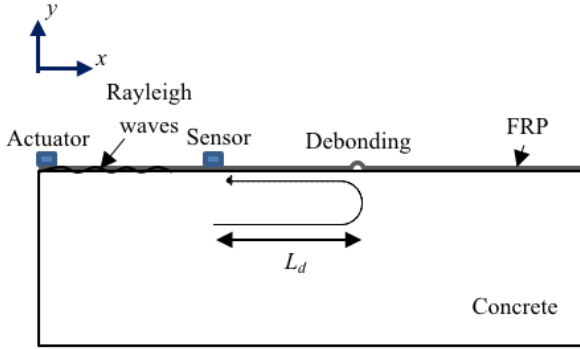


Fig. 2 Schematic diagram of determining damage location in FRP/concrete under one-dimensional situation using ToF

curves for studying guided wave propagation in multi-layered media. In this method, the wave propagation in a bulk material is described and related to displacements and stresses in the material. Then, individual layers would be assembled to create the global matrix representing a complete multi-layered system.

## 2.2 Material properties

The Young's modulus, density and Poisson's ratio of the concrete are assumed to be  $E_c=25$  GPa,  $\rho_c=2400$  kg/m<sup>3</sup> and  $\nu_c=0.16$ , respectively. The FRP composite laminate consists of four plies with layup sequence of (0/90)<sub>s</sub>. The thickness of each lamina is 0.2 mm so that the total thickness of the FRP composite laminates is 0.8 mm. It is assumed that the FRP composite laminate is made up of carbon fibre and epoxy matrix with a fibre weight fraction ( $W_f$ ) of 0.8. Table 1 shows the mechanical properties of the carbon fibre and epoxy matrix. Chamis (1984) formulated mechanical properties of a composite ply based on the properties of fibre and matrix as

$$\rho = V_f \rho_f + V_m \rho_m \quad (1)$$

$$E_{11} = V_f E_{f11} + V_m E_m \quad (2)$$

$$E_{22} = E_{33} = \frac{E_m}{1 - \sqrt{V_f} \left(1 - \frac{E_m}{E_{f22}}\right)} \quad (3)$$

$$G_{12} = G_{13} = \frac{G_m}{1 - \sqrt{V_f} \left(1 - \frac{G_m}{G_{f12}}\right)} \quad (4)$$

$$G_{23} = \frac{G_m}{1 - \sqrt{V_f} \left(1 - \frac{G_m}{G_{f23}}\right)} \quad (5)$$

$$\nu_{12} = \nu_{13} = V_f \nu_{f12} + V_m \nu_m \quad (6)$$

$$\nu_{23} = \frac{E_{22}}{2G_{23}} - 1 \quad (7)$$

where  $V$ ,  $W$ ,  $E$ ,  $G$ ,  $\rho$  and  $\nu$  represent the volume fraction, weight fraction, modulus of elasticity, shear modulus, density and Poisson's ratio of constituent materials, respectively. Also, the subscripts  $f$  and  $m$  denote the properties of fibre and matrix. Based on the elastic properties of carbon fibre and epoxy matrix, and carbon fibre weight fraction, the elastic properties of each FRP ply are calculated and shown in Table 2.

## 2.3 Absorbing regions

Absorbing layers by increasing damping (ALID) is one of the commonly used methods in guided wave problems. It involves adding successive layers to the main structure with gradual increase in damping values while other elastic properties are the same as the main structure. To ensure the explicit FE simulations are computationally efficient, only mass-proportional damping is applied as it only has small effect on stable time increment. Mass-proportional damping across absorbing regions can be formulated as (Rajagopal *et al.* 2012)

$$C_M(x) = C_{Mmax} X(x)^P \quad (8)$$

where  $X(x)$  ranges from 0 at the beginning of absorbing layer and 1 at the end of absorbing layer, and  $C_{Mmax}$  is the maximum mass proportional damping.

## 2.4 Time-of-flight approach for determining debonding location

In this study, a ToF approach is proposed to determine the location of the debonding. ToF-based damage detection techniques have been widely used in guided wave damage detection (Diamanti *et al.* 2005, Soleimanpour and Ng 2017b). Basically, ToF can be defined as the time difference between the incident wave emitted from the actuator and damage-scattered wave captured by the sensor. A simple example is when a debonding is located exactly on the projection of actuator and sensor as shown in Fig. 2.

The sensor captures the incident wave first, and then, the wave reflected from the debonding. Difference of ToF between the reflected wave from the debonding and incident wave ( $\Delta t$ ) can be estimated from the measured data. Since the material properties of the structures are known in advance, and hence, the group velocity of the wave ( $C_g$ ) can be theoretically calculated or it can be directly obtained from experimental measurements. The debonding location can be determined by

$$L_d = \frac{1}{2} (C_g \cdot \Delta t) \quad (9)$$

Fig. 3 illustrates an FRP-retrofitted concrete element with a pair of actuator-sensor attached on FRP retrofitted concrete. The actuator, sensor and debonding are located at  $(x_A, z_A)$ ,  $(x_s, z_s)$  and  $(x_D, z_D)$ , respectively. Eq. (9) can be written as

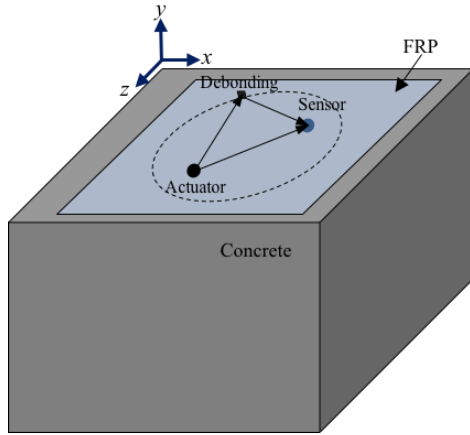


Fig. 3 Schematic diagram of FRP retrofitted concrete with a pair of actuator/sensor

$$\Delta t = t_2 - t_1 = \left( \frac{\sqrt{(x_D - x_A)^2 + (z_D - z_A)^2}}{C_g} + \frac{\sqrt{(x_D - x_S)^2 + (z_D - z_S)^2}}{C_g} - \frac{\sqrt{(x_S - x_A)^2 + (z_S - z_A)^2}}{C_g} \right) \quad (10)$$

where  $t_2$  is arrival time of the signal generated by the actuator, scattered by damage and captured by the sensor while  $t_1$  is arrival time of the wave generated by the actuator and directly captured by the sensor.

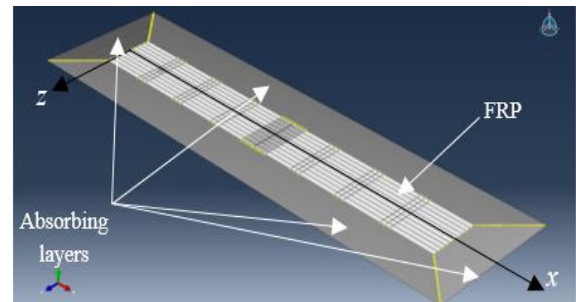
In the real situation, when we have a network of transducers, each of the transducer can be used as both actuator and sensor, Eq. (10) can be further expanded to take into account of this. With a transducer network comprising of  $N_d$  transducers, this relation can be applied to each pair of transducers (actuator and sensor), i.e., transducer ( $i$ ) and transducer ( $j$ ), where  $i, j = 1, 2, \dots, N_d$  and  $i \neq j$ . If  $\Delta t_{i-j}$  denotes difference between arrival time of wave generated by actuator ( $i$ ), and then scattered by damage and captured by sensor ( $j$ ), Eq. (10) then becomes

$$\Delta t_{i-j} = \left( \frac{\sqrt{(x_D - x_i)^2 + (z_D - z_i)^2}}{C_g} + \frac{\sqrt{(x_D - x_j)^2 + (z_D - z_j)^2}}{C_g} - \frac{\sqrt{(x_i - x_j)^2 + (z_i - z_j)^2}}{C_g} \right) \quad (11)$$

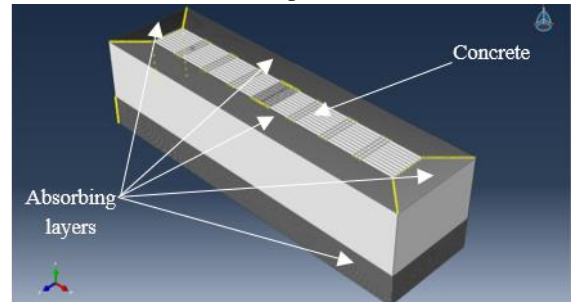
The solution of a set of equations for each actuator-sensor pair results in a number of ellipses and the intersections of elliptic solutions can be used to indicate the debonding location.

Table 3 Comparison between FE and DISPERSE results

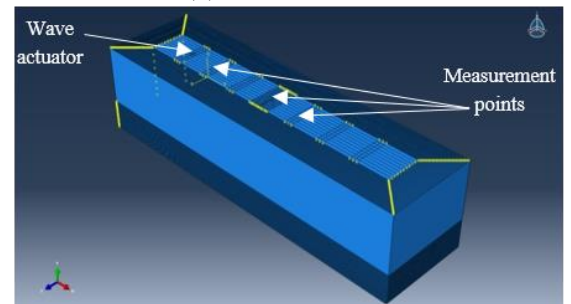
FE				
	$C_x$ (m/s)		$C_y$ (m/s)	
	Out-of-plane excitation	In-plane excitation	Out-of-plane excitation	In-plane excitation
FRP	1517	7478	1138	7553
Concrete	1892		1898	
FRP/concrete	2020		2047	
DISPERSE				
	$C_x$ (m/s)		$C_y$ (m/s)	
	Out-of-plane excitation	In-plane excitation	Out-of-plane excitation	In-plane excitation
FRP	1630	7461	1152	7489
Concrete	1916		1916	
FRP/concrete	2076		2058	



(a) FRP composite model



(b) Concrete model



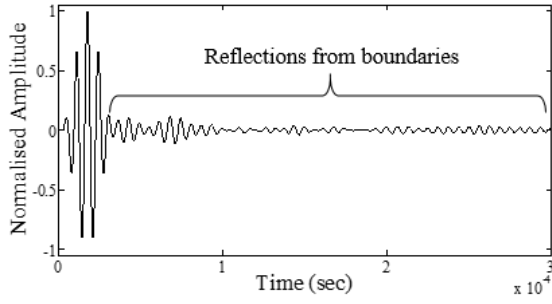
(c) Assembly of FRP-retrofitted concrete

Fig. 4 FE Model 2

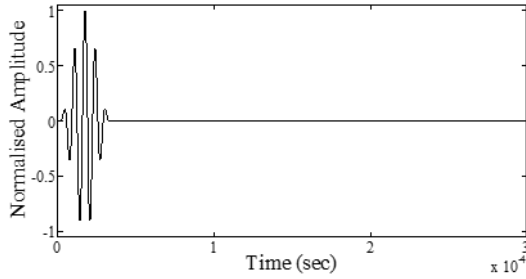
### 3. Results and discussions

#### 3.1 Model verification

To employ the FE simulation of Rayleigh wave for validating the proposed debonding method, the 3D FE model needs to be verified, i.e., the waves simulated in



(a) Model 1 (without absorbing layers)



(b) Model 2 (with absorbing layers)

Fig. 5 Normalised out-of-plane displacement amplitude at  $x=50$  mm and  $z=0$  mm

FRP-retrofitted concrete structure. In the verification, the wave propagation in the FRP composite laminate, concrete and FRP-retrofitted concrete structure are studied individually. The  $3 \times 10^{-4}$ s wave propagation phenomenon is simulated using ABAQUS. Group and phase velocities, which are denoted by  $C_g$  and  $C_p$ , can be calculated as (Aryan *et al.* 2016, Soleimanpour and Ng 2016)

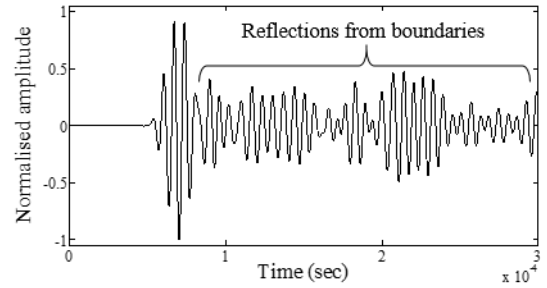
$$C_g = \frac{\Delta x}{\Delta t} \quad (12)$$

$$C_p = \frac{2\pi f_c \Delta x}{\Delta \phi} \quad (13)$$

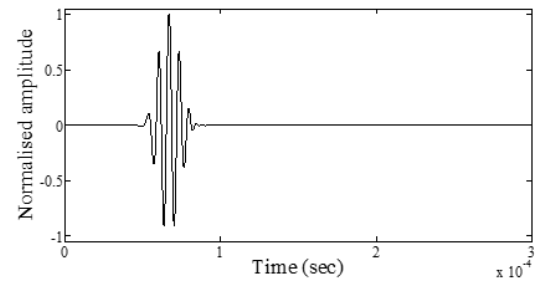
where  $\Delta x$  is distance between measurement points,  $\Delta t$  is difference of wave arrival time,  $f_c$  is the central excitation frequency, and  $\Delta \phi$  indicates phase difference of the wave signals between measurement points. Next, the calculated group and phase velocities are compared with DISPERSER results. In the FRP composite laminate model, in-plane and out-of-plane excitations would result in  $S_0$  and  $A_0$  Lamb wave, respectively. In the concrete and FRP-retrofitted concrete model, both in- and out-of-plane excitations would generate Rayleigh wave. Table 3 shows the calculated group and phase velocities for FRP composite laminate, concrete and FRP/concrete models. There is good agreement between results of FE simulations and DISPERSER.

### 3.2 Implementation of absorbing layers

Absorbing layers are separately applied to the FRP and concrete models. To demonstrate the performance of the absorbing layers in FRP-retrofitted concrete, two models, Model 1 and Model 2, without and with absorbing layers are considered in this study. In both models, the dimensions



(a) Model 1 (without absorbing layers)



(b) Model 2 (with absorbing layers)

Fig. 6 Normalised out-of-plane displacement amplitude at  $x=150$  mm and  $z=0$  mm

of the FRP composite laminate are  $400 \text{ mm} \times 50 \text{ mm}$  ( $L \times W$ ) consisting of four 0.2 mm thick plies with the same mechanical properties and fibre orientation as described in Section 2.2. The dimensions of the concrete in the FE model are  $400 \text{ mm} \times 50 \text{ mm} \times 80 \text{ mm}$  ( $L \times W \times H$ ). Both models are the same except that one of them is without the absorbing layers. In this study, the absorbing region is considered acceptable if the amplitude ratio of reflected wave to incident wave is smaller than -46dB. Considering Eq. (8), a value of  $P$  equal to 3 is used based on the suggestion given by Rajagopal *et al.* (2012). Also, the width of absorbing region is 40 mm and  $C_{Mmax} = 2.5 \times 10^6$ . Rayleigh wave is generated at  $x=50$  mm and  $z=0$  mm based on the Cartesian coordinate as shown in Fig. 4.

To demonstrate the effectiveness of the absorbing region, the calculated out-of-plane displacements are compared between two FRP-retrofitted concrete models, one without and the other with absorbing region. Figs. 5 and 6 show the normalised out-of-plane displacement amplitude at the sensor located at  $x=50$  mm and  $z=0$  mm, and  $x=150$  mm and  $z=0$  mm in Models 1 and 2. As shown in Figs. 5 and 6, absorbing layers have successfully removed boundary reflections reducing the computational cost of simulating Rayleigh in a large size of structure.

### 3.3 Determination of debonding location

A series of numerical case studies are considered, in which the Rayleigh wave simulated by the FRP-retrofitted concrete FE models is used to validate the proposed ToF-based debonding localisation method. In the numerical case studies, the dimensions of the 4-ply FRP are  $250 \text{ mm} \times 200 \text{ mm}$ , which is bonded to a  $250 \text{ mm} \times 200 \text{ mm} \times 80 \text{ mm}$  ( $L \times W \times H$ ) concrete. 40 mm wide ALIDs are applied to the boundaries of FRP and concrete parts. The mechanical properties of the FRP, concrete and absorbing layers are the

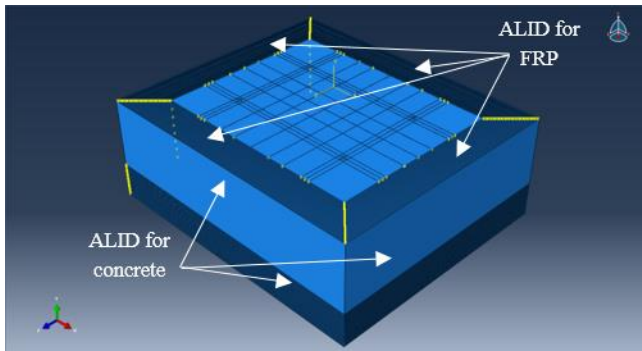


Fig. 7 Assembly of FRP/concrete model

Table 4 Coordinates of the PZT centres in numerical case studies

PZT	x (mm)	z (mm)
1	50	150
2	50	50
3	200	50
4	200	150

Table 5 Coordinates of the debonding centres and diameters in numerical case studies

Case	x (mm)	z (mm)	Debonding diameter (mm)
1	80	120	6
2	125	80	6
3	225	80	6
4	225	80	8

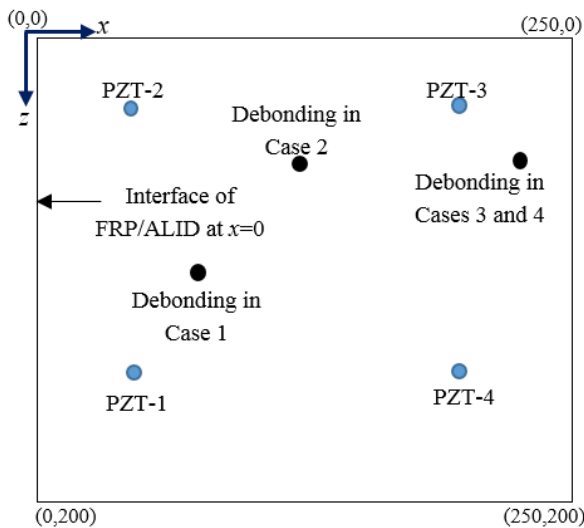
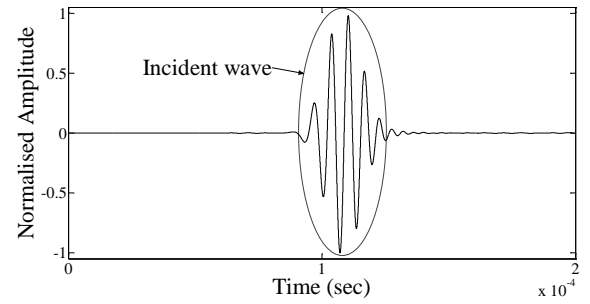
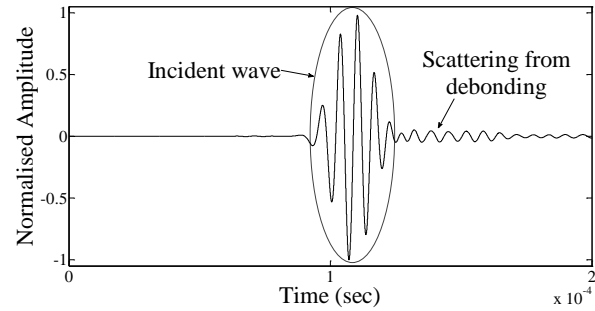


Fig. 8 PZT and debonding locations in Cases 1-3 of the numerical studies

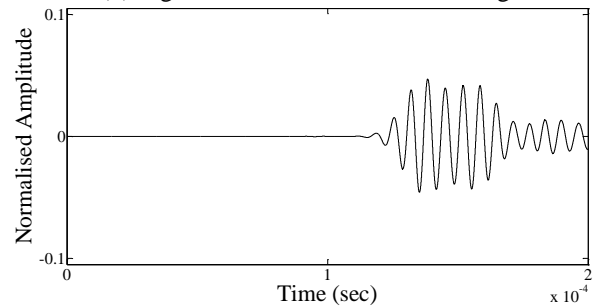
same as those described in Sections 2.2 and 3.2. The assembly of FRP/concrete model is shown in Fig. 7. Four cases are considered in the numerical case studies. Cases 1-3 consider a 6 mm diameter circular debonding located at three different locations as shown in Fig. 8. Based on the Cartesian coordinate shown in Fig. 8, the coordinates of the PZT and the centres of the debondings are summarised in



(a) Signal from model without debonding



(b) Signal from model with debonding



(c) Scattered signal obtained from baseline subtraction

Fig. 9 Wave signals generated by PZT-1 and captured by PZT-3 in the model without rebars

Tables 4 and 5, respectively. Case 4 considers a debonding at the same location as Case 3 but the diameter of the debonding is increased to 8 mm.

In each case, Rayleigh wave is sequentially generated by each PZT, and at the same time the wave signals are measured by the rest of the PZTs. A model without the debonding is used for baseline subtracting purpose to extract the scattered wave signal. The scattered wave is obtained by subtracting the simulated displacement responses of the model with debonding from those of the intact model. Rayleigh wave signals are normalised based on the maximum absolute amplitude of signal in the model without debonding. Fig. 9(a) shows the incident wave generated by PZT-1 and captured at PZT-3 in the model without debonding in Case 4. Fig. 9(b) presents wave generated by PZT-1, scattered at the debonding and then captured by PZT-3. The scattered signal is shown in Fig. 9(c).

As discussed in Section 2.1, rebars have minor effects on incident Rayleigh waves and rebar reflections can be removed by the baseline subtraction. To demonstrate the effect of rebar in wave propagation, 10 mm diameter steel bars with a concrete cover of 50 mm are added to the FE

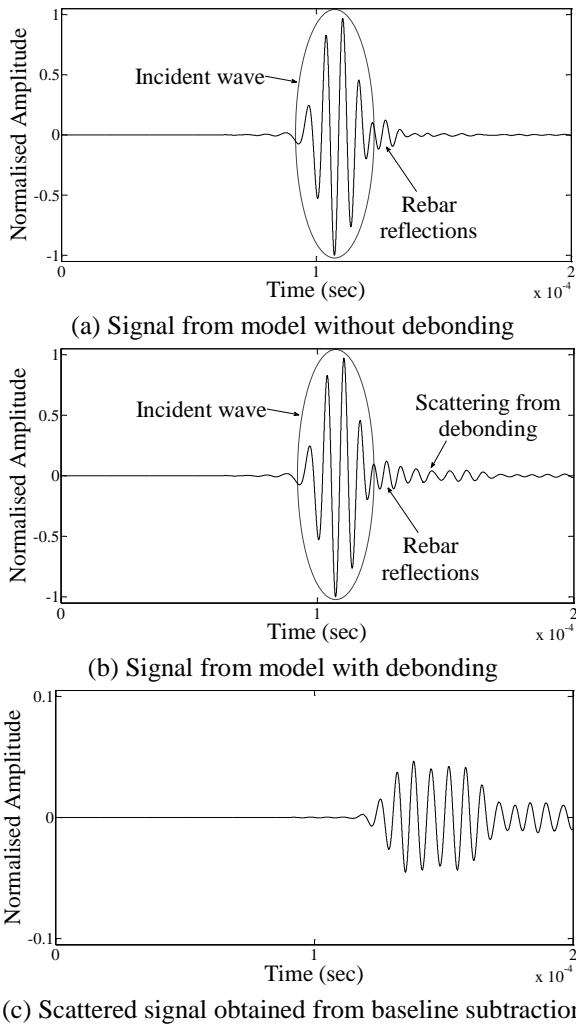


Fig. 10 Wave signals generated by PZT-1 and captured by PZT-3 in the model with rebars

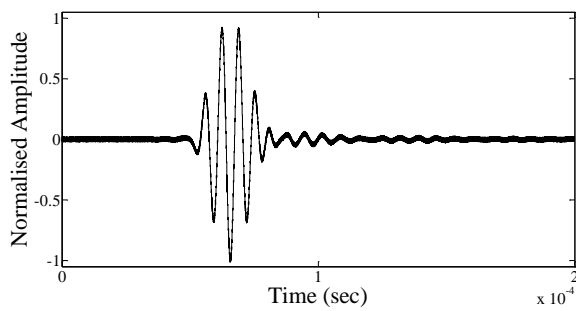


Fig. 11 Wave signals generated by PZT-4 and captured by PZT-3 for debonding Case 4

model. Fig. 10(a) displays the incident wave generated by PZT-1 and captured at PZT-3 in the model with rebar and without debonding between FRP and concrete. Fig. 10(b) shows the wave signal generated by PZT-1, scattered at the debonding and then captured by PZT-3. The scattered signal from debonding in the model with rebars is shown in Fig. 10(c). As seen in Figs. 9(c) and 10(c), the scattered signal is the same for both models, i.e., without and with rebars. It should be noted that experimentally measured Rayleigh wave signals contain some degrees of noise. The

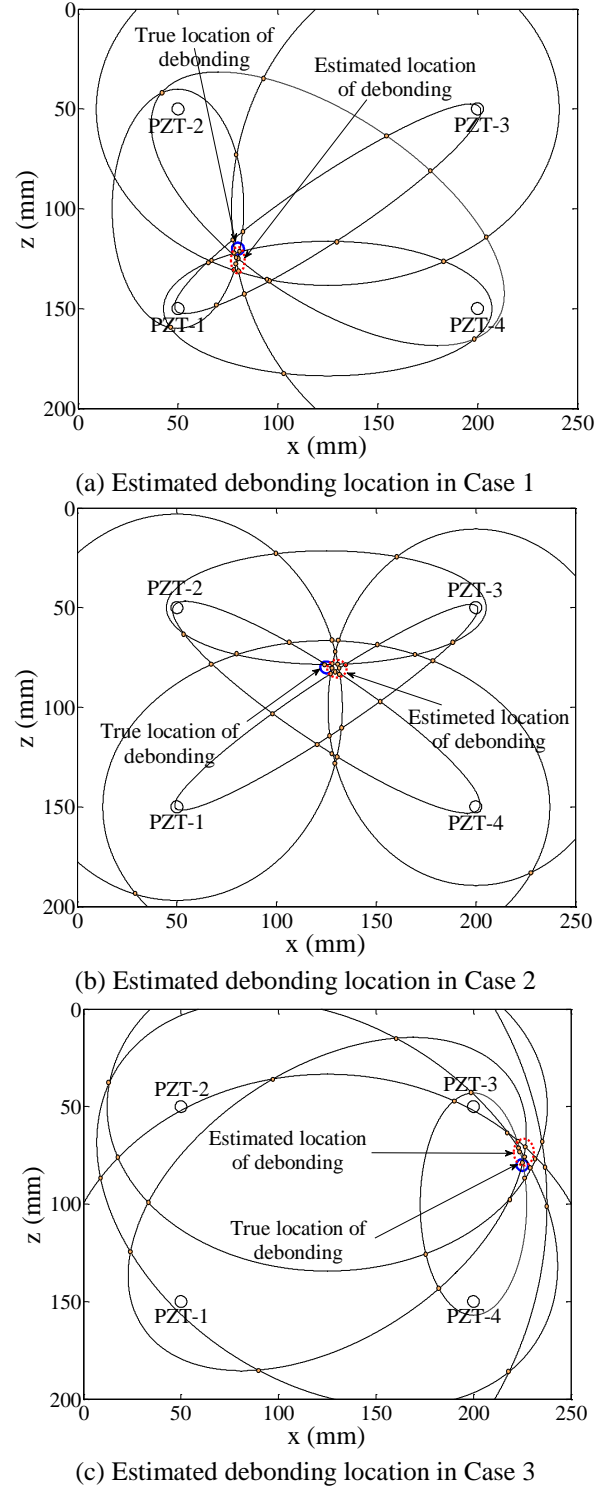


Fig. 12 Elliptic solutions for 6 mm diameter circular debonding in Cases 1-3

quality of signals can be improved significantly by averaging and also applying a bandpass filter. Thus, for numerical case studies of damage localisation, 2% of noise was added to the signals obtained from FE simulations. That could ensure that the proposed method can be used in practical situations. Figure 11 shows the signal generated by PZT-4 and captured by PZT-3 for debonding case 4 with the added noise.

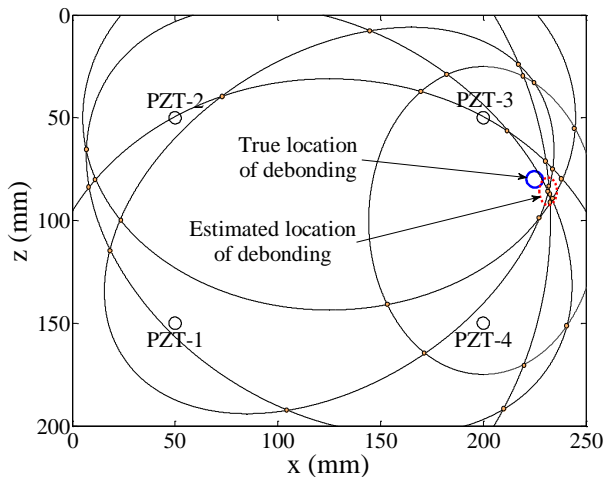


Fig. 13 Elliptic solutions for 8 mm diameter circular debonding in Case 4

The ToF is calculated based on the difference of arrival time of incident wave and the scattered wave from the debonding. Elliptic solutions of Cases 1-3 are obtained based on Eq. (11) for each debonding location and are shown in Figs. 12(a)-(c), respectively. The intersection of each pair of ellipses is indicated by a solid circle. The area with the highest concentration of circles, as indicated by an ellipse with red dotted line, is the most probable location of the debonding. The true debonding location and size are indicated by circles with solid blue line.

To validate the proposed ToF-based damage localisation method for larger size of debonding, Case 4 considers an 8 mm diameter circular debonding located at the same location as the debonding in Case 3. The elliptic solution for this case is shown in Fig. 13. As shown in Figs. 12 and 13, the ToF-based damage localisation method is successfully applied to detect debonding at FRP/concrete interface in the numerical case studies.

#### 4. Conclusions

A damage detection method has been proposed to determine the debonding location in the FRP-retrofitted concrete structures. The proposed method locates the debonding based on the ToF information of the incident Rayleigh wave and scattered wave from the debonding. In this study, the 3D FE model has been developed to simulate Rayleigh wave generated by piezoelectric transducers in the FRP-retrofitted concrete structures and wave scattering at debondings. Analytical solutions have been adopted to verify the FE simulations of Rayleigh wave propagation in the FRP-retrofitted concrete structures. It has been shown that Rayleigh wave is sensitive to the debonding between FRP and concrete. Absorbing layers have been successfully applied to the FE model to reduce the computational cost in the numerical case studies for verifying the proposed debonding detection method. It has been shown that the proposed ToF-based debonding detection method is able to accurately locate the debonding in the FRP-retrofitted concrete structures.

#### Acknowledgments

This work was supported by the Australian Research Council (ARC) under Grant Number DE130100261. The support is greatly appreciated

#### References

- ACI 440R (2007), *Report on Fiber-Reinforced Polymer (FRP) Reinforcement for Concrete Structures*, ACI Committee 440, American Concrete Institute, Farmington Hills, Michigan, U.S.A.
- Aggelis, D.G. and Shiotani, T. (2007), "Repair evaluation of concrete cracks using surface and through-transmission wave measurements", *Cement Concrete Compos.*, **29**, 700-711.
- Aggelis, D.G., Shiotani, T. and Polyzos, D. (2009), "Characterization of surface crack depth and repair evaluation using rayleigh waves", *Cement Concrete Compos.*, **31**, 77-83.
- Akuthota, B., Hughes, D., Zoughi, R., Myers, J. and Nanni, A. (2004), "Near-field microwave detection of disbond in carbon fiber reinforced polymer composites used for strengthening cement-based structures and disbond repair verification", *J. Mater. Civil Eng.*, **16**, 540-546.
- Alampalli, S. and Ettouney, M.M. (2014), *Structural Health Monitoring, the International Handbook of FRP Composites in Civil Engineering*, CRC Press, Boca Raton, Florida, U.S.A.
- Aryan, P., Kotousov, A., Ng, C.T. and Cazzolato, B. (2017a), "A model-based method for damage detection with guided waves", *Struct. Contr. Health Monitor.*, **24**(3), e1884.
- Aryan, P., Kotousov, A., Ng, C.T. and Cazzolato, B.S. (2017b), "A Baseline-free and non-contact method for detection and imaging of structural damage using 3D laser vibrometry", *Struct. Contr. Health Monitor.*, **24**(4), e1894.
- Aryan, P., Kotousov, A., Ng, C.T. and Wildy, S. (2016), "Reconstruction of baseline time-trace under changing environmental and operational conditions", *Smart Mater. Struct.*, **25**(3), 035018.
- Balaguru, P., Nanni, A. and Giancaspro, J. (2009), *FRP Composites for Reinforced and Prestressed Concrete Structures: A Guide to Fundamentals and Design for Repair and Retrofit*, Taylor and Francis, New York, U.S.A.
- Bank, L.C. (2006), *Composite for Construction: Structural Design with FRP Materials*, John Wiley and Sons, Hoboken, New Jersey, U.S.A.
- Biolzi, L., Ghittoni, C., Fedele, R. and Rosati, G. (2013), "Experimental and theoretical issues in FRP-concrete bonding", *Constr. Build. Mater.*, **41**, 182-190.
- Brown, J.R. and Hamilton, H.R. (2013), "Quantitative infrared thermography inspection for FRP applied to concrete using single pixel analysis", *Constr. Build. Mater.*, **38**, 1292-1302.
- Carboni, M., Giannelis, A. and Giglio, M. (2015), "A Lamb waves based statistical approach to structural health monitoring of carbon fibre reinforced polymer composites", *Ultrason.*, **60**, 51-64.
- Chakraborty, A. (2009), *Modeling of Lamb Waves in Composite Structures*, Encyclopedia of Structural Health Monitoring, John Wiley and Sons.
- Chamis, C.C. (1984), *Mechanics of Composite Materials: Past, Present and Future*, NASA Technical Memorandum, 100793.
- Cheeke, J.D.N. (2012), *Fundamentals and Applications of Ultrasonic Waves*, CRC Press, Boca Raton, Florida, U.S.A.
- Choi, E., Utui, N. and Kim, H.S. (2013), "Experimental and analytical investigations on debonding of hybrid FRPs for flexural strengthening of RC beams", *Compos. Part B*, **45**, 248-256.

- D'Antino, T. and Pellegrino, C. (2014), "Bond between FRP composites and concrete: Assessment of design procedures and analytical models", *Compos. Part B*, **60**, 440-456.
- Diamanti, K., Hodgkinson, J.M. and Soutis, C. (2004), "Detection of low-velocity impact damage in composite plates using lamb waves", *Struct. Health Monitor.*, **3**(1), 33-41.
- Diamanti, K., Soutis, C. and Hodgkinson, J.M. (2005), "Lamb waves for the non-destructive inspection of monolithic and sandwich composite beams", *Compos. Part A*, **36**, 189-195.
- Edwards, R.S., Dixon, S. and Jian, X. (2006), "Depth gauging of defects using low frequency wideband Rayleigh waves", *Ultrason.*, **44**, 93-98.
- Etounney, M.M. and Alampalli, S. (2012), *Infrastructure Health in Civil Engineering: Application and Management*, CRC Press, Boca Raton, Florida, U.S.A.
- Fam, A. and Mirmiran, A. (2014), *QA/QC, Maintenance, and Repair of Hybrid Structures*, The International Handbook of FRP Composites in Civil Engineering, CRC Press, Boca Raton, Florida, U.S.A.
- Harb, M.S. and Yuan, F.G. (2015), "A rapid, fully non-contact, hybrid system for generating lamb wave dispersion curves", *Ultrason.*, **61**, 62-70.
- He, S. and Ng, C.T. (2015), "Analysis of mode conversion and scattering of guided waves at cracks in isotropic beams using a time-domain spectral finite element method", *Electr. J. Struct. Eng.*, **14**(1), 20-32.
- He, S. and Ng, C.T. (2016), "A probabilistic approach for quantitative identification of multiple delamination in laminated composite beams using guided waves", *Eng. Struct.*, **127**, 602-614.
- He, S. and Ng, C.T. (2017a), "Guided wave-based identification of multiple cracks in beam using a bayesian approach", *Mech. Syst. Sig. Proc.*, **84**, 324-345.
- He, S. and Ng, C.T. (2017b), "Modelling and analysis of nonlinear guided waves interaction at a breathing crack using time-domain spectral finite element method", *Smart. Mater. Struct.*, **26**, 085002.
- Hedayatrasa, S., Abhary, K., Uddin, M. and Ng, C.T. (2016), "Optimum design of phonic crystal perforated plate structures for widest bandgap of fundamental guided wave modes and maximized in-plane stiffness", *J. Mech. Phys. Sol.*, **89**, 31-58.
- Hevin, G., Abraham, O., Pedersen, H.A. and Campillo, M. (1998), "Characterisation of surface cracks with Rayleigh waves: A numerical model", *NDT E Int.*, **31**(4), 289-297.
- Jiang, T., Kong, Q., Patil, D., Luo, Z., Huo, L. and Song, G. (2017), "Detection of debonding between fiber reinforced polymer bar and concrete structure using piezoceramic transducers and wavelet packet analysis", *IEEE Sens. J.*, **17**(7), 1992-1998.
- Karbhari, V.M., Kaiser, H., Navada, R., Ghosh, K. and Lee, L. (2005), *Methods for Detecting Defects in Composite Rehabilitated Concrete Structures*, Oregon Department of Transportation, and Federal Highway Administration, U.S.A.
- Khan, M.A. (2010), *Bridge and Highway Structure Rehabilitation and Repair*, McGraw-Hill, New York, U.S.A.
- Ko, H., Matthys, S., Palmieri, A. and Sato, Y. (2014), "Development of a simplified bond stress-slip model for bonded FRP-concrete interfaces", *Constr. Build. Mater.*, **68**, 142-157.
- Luo, M., Li, W., Hei, C. and Song, G. (2016), "Concrete infill monitoring in concrete-filled FRP tubes using a PZT-based ultrasonic time-of-flight method", *Sens.*, **16**(12), 1-11.
- Mirmiran, A., Shahawy, M. and Echary, H.E. (1999), "Acoustic emission monitoring of hybrid FRP-concrete columns", *J. Eng. Mech.*, **125**(8), 899-905.
- Mohabuth, M., Kotousov, A. and Ng, C.T. (2016), "Effect of uniaxial stress on the propagation of higher-order lamb wave modes", *J. Nonlin. Mech.*, **86**, 104-111.
- Nassr, A.A. and Dakhkhni, W.W.E. (2009), "Damage detection of FRP-strengthened concrete structures using capacitance measurements", *J. Compos. Constr.*, **13**(6), 486-497.
- Ng, C.T. (2014a), "Bayesian model updating approach for experimental identification of damage in beams using guided waves", *Struct. Health Monitor.*, **13**(4), 359-373.
- Ng, C.T. (2014b), "On the selection of advanced signal processing techniques for guided wave damage identification using a statistical approach", *Eng. Struct.*, **67**, 50-60.
- Ng, C.T. (2015a), "On accuracy of analytical modeling of Lamb wave scattering at delaminations in multilayered isotropic plates", *J. Struct. Stab. Dyn.*, **15**(7), 1-12.
- Ng, C.T. (2015b), "A two-stage approach for quantitative damage imaging in metallic plates using lamb waves", *Earthq. Struct.*, **8**(4), 821-841.
- Ng, C.T. and Chan, T.H.T. (2014), "Special issue on structural health monitoring of civil structures", *Struct. Health Monitor.*, **13**(4), 345-346.
- Nishizaki, I. and Meiarashi, S. (2002), "Long-term deterioration of GFRP in water and moist environment", *J. Compos. Constr.*, **6**(1), 21-27.
- Pavlakovic, B. and Lowe, M. (2003), *DISPERSE Version 2.0.16 User's Manual*, Imperial College NDT Laboratory, U.K.
- Raghavan, A. and Cesnik, C.E.S. (2007), "Review of guided-wave structural health monitoring", *Shock Vib. Dig.*, **39**(2), 91-114.
- Rajagopal, P., Drozd, M., A.Skelton, E., Lowe, M.J.S. and Craster, R.V. (2012), "On the use of absorbing layers to simulate the propagation of elastic waves in unbounded isotropic media using commercially available Finite Element packages", *NDT E Int.*, **51**, 30-40.
- Ramadas, C., Balasubramaniam, K., Joshi, M. and Krishnamurthy, C.V. (2009), "Interaction of the primary anti-symmetric Lamb mode ( $A_0$ ) with symmetric delaminations: Numerical and experimental studies", *Smart Mater. Struct.*, **18**, 1-7.
- Ramadas, C., Balasubramaniam, K., Joshi, M. and Krishnamurthy, C.V. (2010), "Interaction of guided lamb waves with an asymmetrically located delamination in a laminated composite plate", *Smart Mater. Struct.*, **19**, 1-11.
- Rose, J.L. (2002), "A baseline and vision of ultrasonic guided wave inspection potential", *J. Press. Vess. Technol.*, **124**, 273-282.
- Schubert, K.J., Brauner, C. and Herrmann, A.S. (2014), "Non-damage-related influences on lamb wave-based structural health monitoring of carbon fiber-reinforced plastic structures", *Struct. Health Monitor.*, **13**(2), 158-176.
- Sevillano, E., Sun, R., Perera, R., Arteaga, A., De Diego, A. and Cisneros, D. (2016), "Comparison of PZT and FBG sensing technologies for debonding detection on reinforced concrete beams strengthened with external CFRP strips subjected to bending loads", *Mater. Constr.*, **66**(322), 1-12.
- Shin, S.W., Yun, C.B., Popovics, J.S. and Kim, J.H. (2007), "Improved rayleigh wave velocity measurement for nondestructive early-age concrete monitoring", *Res. Nondestr. Eval.*, **18**, 45-68.
- Singh, R.K., Ramadas, C., Misal, R.D. and Thakur, D.G. (2012), "Numerical analysis of lamb wave propagation in delaminated composite laminate", *Proc. Eng.*, **380**, 2510-2519.
- Soleimanpour, R. and Ng, C.T. (2016), "Scattering characteristics of the fundamental anti-symmetric lamb wave at cracks in isotropic plates", *J. Civil Struct. Health Monitor.*, **6**(3), 447-459.
- Soleimanpour, R. and Ng, C.T. (2017a), "Higher harmonic generation of guided waves at delaminations in laminated composite beams", *Struct. Health Monitor.*, **16**(4), 400-417.
- Soleimanpour, R. and Ng, C.T. (2017b), "Locating delaminations in laminated composite beams using nonlinear guided waves", *Eng. Struct.*, **131**, 207-219.

- Sun, M., Staszewski, W.J., Swamy, R.N. and Li, Z. (2008), "Application of low-profile piezoceramic transducers for health monitoring of concrete structures", *NDT E Int.*, **41**(8), 589-595.
- Sun, R., Sevillano, E. and Perera, R. (2015), "Debonding detection of FRP strengthened concrete beams by using impedance measurements and an ensemble PSO adaptive spectral model", *Compos. Struct.*, **125**, 374-387.
- Tian, Z., Yu, L. and Leckey, C. (2015), "Delamination detection and quantification on laminated composite structures with lamb waves and wavenumber analysis", *J. Intell. Mater. Syst. Struct.*, **26**(13), 1723-1738.
- Turatsinze, A., Beushausen, H., Gagné, R., Granju, J.L., Silfwerbrand, J. and Walter, R. (2011), *Bonded Cement-Based Material Overlays for the Repair, the Lining or The Strengthening of Slabs or Pavements*, Springer, Dordrecht, the Netherlands.
- Washer, G.A. and Alampalli, S. (2014a), *Nondestructive Evaluation Methods for Composite Materials: General Overview, Visual Inspection, and Microwave Methods*, the International Handbook of FRP Composites in Civil Engineering, CRC Press, Boca Raton, Florida, U.S.A.
- Washer, G.A. and Alampalli, S. (2014b), *Nondestructive Evaluation Methods for Composite Materials: Infrared Thermography*, the International Handbook of FRP Composites in Civil Engineering, CRC Press, Boca Raton, Florida, U.S.A.
- Worden, K., Farrar, C.R., Manson, G. and Park, G. (2007), "The fundamental axioms of structural health monitoring", *Proc. Trans. R. Soc. A*, **463**, 1639-1664.
- Wu, F. and Chang, F.K. (2006), "Debond detection using embedded piezoelectric elements for reinforced concrete structures-part II: Analysis and algorithm", *Struct. Health Monitor.*, **5**(1), 17-28.
- Xu, Y., Leung, C.K.Y., Tong, P., Yi, J. and Lee, S.K.L. (2005), "Interfacial debonding detection in bonded repair with a fiber optical interferometric sensor", *Compos. Sci. Technol.*, **65**(9), 1428-1435.
- Yang, Y., Ng, C.T., Kotousov, A., Sohn, H. and Lim, H.J. (2018), "Second harmonic generation at fatigue cracks by low-frequency lamb waves: Experimental and numerical studies", *Mech. Syst. Sig. Proc.*, **99**, 760-773.
- Zerwer, A., Polak, M.A. and Santamarina, J.C. (2005), "Detection of surface breaking cracks in concrete members using rayleigh waves", *J. Environ. Eng. Geophys.*, **10**(3), 1-12.